Influence of Local Flow Acceleration on the Heat Transfer of Submerged and Free-surface Jet Impingement

Conference Paper · August 2014

DOI: 10.1615/IHTC15.fcv.008378

CITATIONS
6

READS
248

5 authors, including:

Wilko Rohlfs
University of Twente
73 PUBLICATIONS **690** CITATIONS
SEE PROFILE

Claas Ehrenpreis
RWTH Aachen University
15 PUBLICATIONS **54** CITATIONS
SEE PROFILE

Herman D. Haustein
Tel Aviv University
44 PUBLICATIONS **325** CITATIONS
SEE PROFILE

Oliver Garbrecht
RWTH Aachen University
12 PUBLICATIONS **179** CITATIONS
SEE PROFILE

Proceedings of the 15th International Heat Transfer Conference, IHTC-15
August 10-15, 2014, Kyoto, Japan

IHTC15-8378

INFLUENCE OF LOCAL FLOW ACCELERATION ON THE HEAT TRANSFER OF SUBMERGED AND FREE-SURFACE JET IMPINGEMENT

W. Rohlfs,[1,*] C. Ehrenpreis,[1] H. D. Haustein,[1] O. Garbrecht,[1] R. Kneer[1]

[1]Institute of Heat and Mass Transfer, RWTH Aachen University, Aachen, 52056, Germany

ABSTRACT

The present study of low Reynolds number submerged and free-surface jet impingement examines the cause of peaks in the radial distribution of the Nusselt number by way of fully resolved numerical simulation. In a first step, the flow behavior of free-surface and submerged free jets is examined, revealing a different development of the initial velocity profile while traveling towards the impingement wall. The shape of the Nusselt distribution is found to be significantly influenced by the velocity profile close to the wall, however, showing similar trends for both, submerged and free-surface jets. Thus, a local peak in the heat transfer distribution is found to exist not only for submerged but also for free-surface jets under specific conditions (long nozzle-to-plate distances and low Reynolds numbers). The causing effect of the local peak is revealed in detail, showing that local flow acceleration in radial direction is the dominant cause for the increasing heat transfer coefficient in flow direction.

KEY WORDS: laminar jet impingement, free-surface jet, submerged jet, local flow acceleration

1. INTRODUCTION

Impinging jets are gaseous or liquid flows released against a surface and are characterized by high heat and mass transfer rates. They are commonly employed in heating, cooling or drying [25]. In the last few decades, many experimental and numerical investigations have been conducted on this topic. A distinction between two types of jets can be made if a liquid is used as a working fluid: Submerged jets, in which case a liquid is issued into a liquid and free-surface jets, in which a liquid jet entrains a gaseous atmosphere. Comprehensive surveys focussing on submerged jets are presented by various authors [14, 27, 29].

Traditionally, the heat transfer for jet impingement is described by three dimensionless parameters: the Reynolds number, $Re = uD/\nu$, the Prandtl number, $Pr = \nu/a$, and the nozzle-to-plate distance, H/D (where ν, a, u, and D denote the viscosity, thermal diffusivity, average velocity, and nozzle diameter, respectively). Typical correlations for the dimensionless heat transfer (dimensionless heat transfer coefficient) for both free-surface and submerged jets are of the form

$$Nu = \frac{h \cdot D}{k} = C \cdot Pr^{\alpha} Re^{\beta} \left(\frac{H}{D}\right)^{\gamma} \tag{1}$$

, where k and h denote the thermal conductivity and convective heat transfer coefficient, respectively. The constants in the correlation, C, α, β, and γ, are determined using experimental data and vary in the literature.

*Corresponding W. Rohlfs: rohlfs@wsa.rwth-aachen.de

From the exact solution of boundary layer or stagnation flow problem, analytical Prandtl number dependencies can be deduced [23, 28]. This dependency has also been applied in the analytical work of Ma et al. [13], describing the heat transfer of liquid jet impingement based on simplified boundary layer equations as previously done by Liu and Lienhard [10]. In a recent study by the authors [19], numerical simulation results for $0.07 < Pr < 1300$ have revealed excellent agreement with the analytical Prandtl number dependency in the stagnation region.

Regarding the Reynolds number dependency, values in the range of $0.4 < \beta < 0.873$ were found in experimental investigations [1, 26], whereby lower values are usually associated with laminar and higher values with turbulent flow conditions. Analytical solutions [13, 26] and many experimental studies suggest a dependency around $\beta = 0.5$, a scaling well known from laminar boundary layer theory [23]. The nozzle-to-plate distance H/D strongly affects submerged impinging jets, where the surrounding liquid decelerates the jet rapidly through strong shear forces. For free-surface jets, correlations reported in several studies [6, 26] suggest a weak dependency on H/D with an exponent ranging from $\gamma = -0.0336$ to $\gamma = -0.105$. Based on numerical simulations, it has recently been shown by the authors that the extent of viscous relaxation during the free-jet flight, which changes the shape of the velocity profile initially emerging from the nozzle, can be described by a dimensionless time scale, $H/(D \cdot Re)$. Using this time scale, a self-similar description of the velocity profile in axial and radial directions and consequently a self-similar description of the heat transfer coefficient for laminar flow conditions has been proposed [19].

An important classification is the distinction between laminar and turbulent jets. More specifically, circular jets can be attributed to four classifications [17]: Dissipated laminar jets, for $Re < 300$, fully laminar jets, $300 < Re < 1000$, a transition region or semi-turbulent jets, $1000 < Re < 3000$ and fully turbulent jets for $Re > 3000$. However, other factors such as the velocity profile, the separation distance, and whether the jet is confined or not may lead to an earlier or delayed transition from laminar to turbulent jets with respect to the Reynolds number [17]. The present study investigates laminar jets up to a Reynolds number of 2000, not accounting for three-dimensional turbulent effects, due to the assumption of axial symmetry in the numerical method.

The setup investigated in the present study is shown in Fig. 1 (top). The jet emerges from the nozzle and impinges on the plate after a nozzle-to-plate distance of h/D, thereby cooling the heated wall. The local Nusselt number (dimensionless heat transfer coefficient) of free-surface and submerged axisymmetric impinging jets can generally be characterized by a high value at the centerline with a monotonic decrease in the radial direction. However, the existence of local peaks in the radial Nusselt number profile has been observed for submerged jets [5, 12, 18] (see Fig. 1, bottom). Those peaks have been identified to occur at two dominant locations: The *inner peak* occurring in the vicinity of the outer edge of the incoming jet ($r/D = 0.5$) and an *outer peak* which occurs at a distance of about two nozzle diameters downstream.

Several plausible explanations for the two peaks have been proposed in the literature. Both peaks have been investigated by the authors for the submerged jet configuration in an earlier study [20]. We refer to this article for a detailed discussion of the outer peak. As the present study extends the investigation of the inner peak to free-surface jets, the possible explanations for this peak shall be revealed shortly: Gardon and Akfirat [5] have suggested that local flow acceleration at nozzle-plate spacings up to $h/D = 3$ and local thinning of the boundary layer are the causes for the increase in Nusselt number. They observed the inner peak for Reynolds numbers as low as 2500 and thus concluded that turbulence can only play a minor role. This has previously also been found in the theoretical analysis by Kezios [9]. In contrast, Pamadi and Belov [15] have suggested that the inner peak is attributed to the penetration of the maximal turbulence into the boundary layer, occurring at the outer edge of the incoming jet. They based their results on a solution of the incompressible flow parabolic equations that included a turbulence model. Lytle and Webb [12] also suggested that the inner peak is associated with a significant increase in turbulence. However, this theory stands in contrast to the findings of Gardon and Akfirat [5], mentioned above. A further explanation is given by Kataoka et al. [8], suggesting that the inner peak is actually caused by the impingement of large vortices on the wall, which arise at the outer edge of the

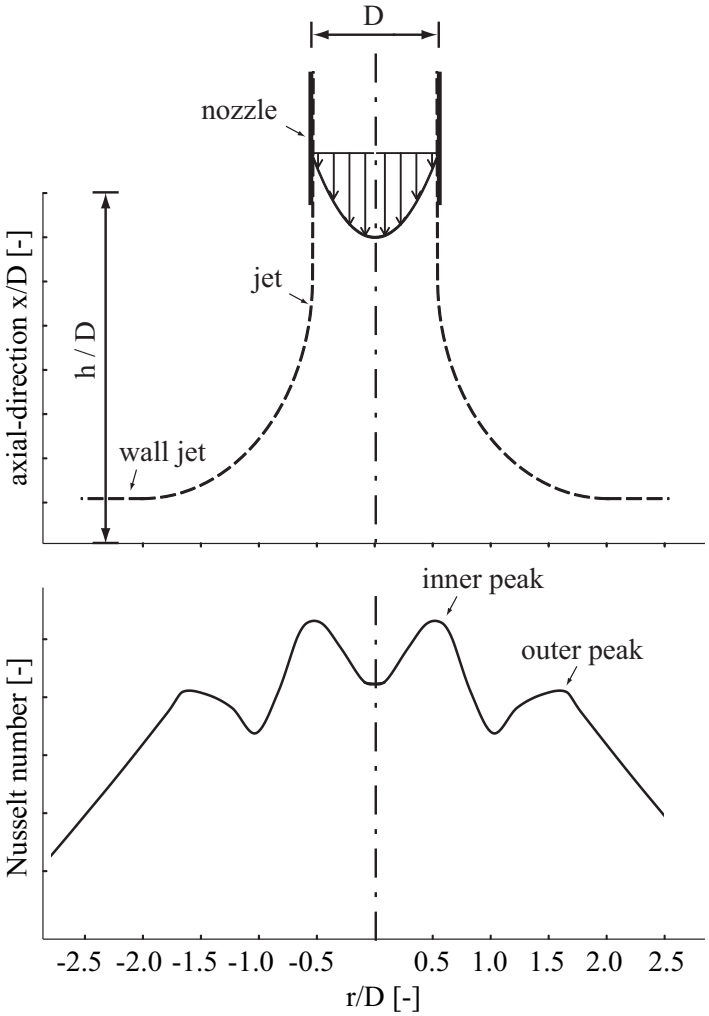

Fig. 1 Visualization of the setup.

jet. In a numerical study by Saad et al. [22], the influence of two different inlet velocity profiles – parabolic and uniform – has been investigated. For the case of a uniform-velocity profile, the inner peak was found at Reynolds numbers of 950 and 1960, for which its location coincided with the location of maximal skin friction. They also found that the velocity profile has a strong influence on the heat transfer characteristics at the point of impingement.

In a former study by the authors [20], the origin of the inner peak was shown to be associated to the occurrence of local flow acceleration and not necessarily to the occurrence of turbulence. An increase of the radial acceleration in radial direction, causing an inflow toward the wall, revealed to be the key explanation for the inner peak. As this acceleration is caused by the pressure gradient in the stagnation region, the shape of the velocity profile at the nozzle exit was found to dictate the existence of a local peak. This also explaines why the inner peak has previously been associated with higher Reynolds numbers and lower nozzle-to-wall distances, in which case the necessary pressure gradient is achieved.

The present study focusses on the investigation of laminar submerged and free-surface jet impingement. The hydrodynamics of free jets is examined, first for the two different jet configurations and for uniform and parabolic inlet velocity profiles. In a second step, the heat transfer characteristics of both jet types are presented. The effect of local flow acceleration is discussed for the case of free-surface jets.

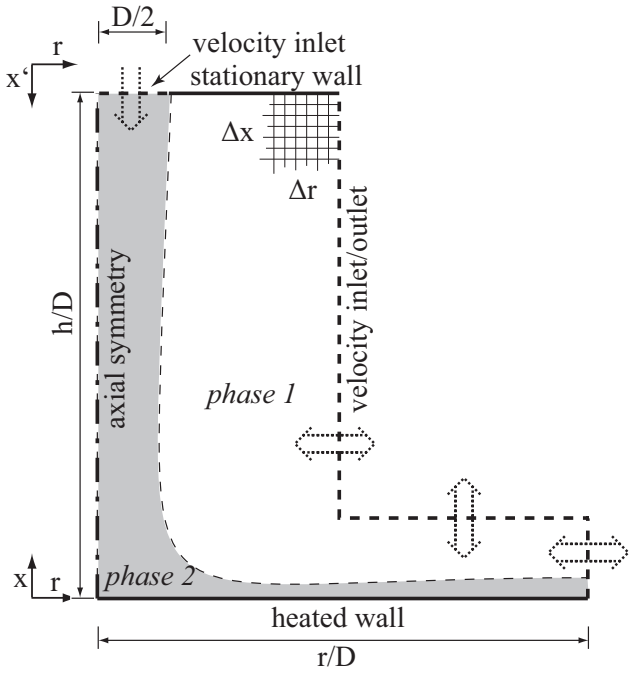

Fig. 2 Computational domain: For the free jet case, phase 1 and phase 2 are immiscible while for the submerged jet case only one phase exists.

2. NUMERICAL METHOD

The numerical simulations of the free and submerged jet configuration are performed by solving the full incompressible Navier-Stokes equations with the finite volume method with axisymmetric boundary conditions. The multiphase character of the free jet configuration is accounted for by the volume of fluid (VOF, [7]) and continuum surface force method (CSF, [3]). These methods are implemented in the *interFOAM* solver of the CFD-solver package OpenFOAM [21] that was applied in this study. For the coupling between momentum and mass conservation, the pressure implicit solution method (PISO) is applied, while for the temperature, a scalar transport equation is solved. The density and viscosity ratio between phase 1 and phase 2 is $\rho_1/\rho_2 = 1.6 \cdot 10^{-3}$ and $\nu_1/\nu_2 = 0.129$, respectively. No back coupling between the temperature and the velocity or pressure, e.g. by buoyancy forces or temperature-dependent thermophysical properties, is accounted for. Thus, the simulation results correspond to cases where the temperature change of the fluid is sufficiently low and the assumption of constant fluid properties remains valid. This leads to two limitations. First, the temperature difference between the fluid and the wall has to be low, which does not affect the dimensionless consideration of the problem. Second, the dissipative heat generation, which is not accounted for in the numerical simulations, and consequently a temperature increase in the near wall region caused by dissipation has to be small compared to the thermal dependency of the fluid properties.

The central differences scheme is used for all spatial discretization and a first order, bounded implicit scheme is applied for temporal discretization. The computational domain (see Fig. 2) consists of two parallel walls, the lower heated wall on which the jet impinges and the upper wall, through which the jet emerges.

The computational domain is spatially discretized by hexahedral cells with a cell size in the radial direction of $9 \cdot 10^{-4} D \leq \Delta r \leq 0.1D$. The cell size in the axial direction near the wall corresponds to one-tenth of the characteristic viscous length scale (which is the maximum value of $y^+ = 0.12$ for the highest Reynolds number). The resulting number of cells ranges from 80,400 to 131,800.

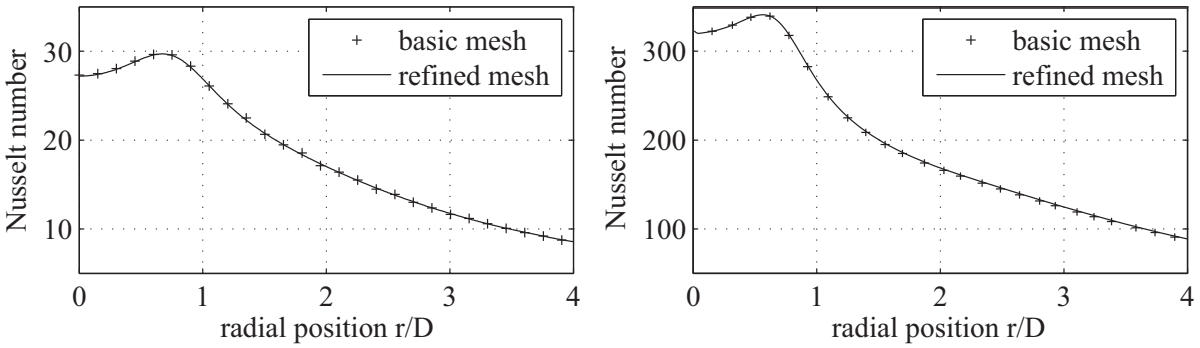

(a) Submerged jet: $Re = 1804$ and $Pr = 0.72$ (b) Free-surface jet: $Re = 793$ and $Pr = 1307$

Fig. 3 Grid dependence analysis. Nusselt number distribution at the wall.

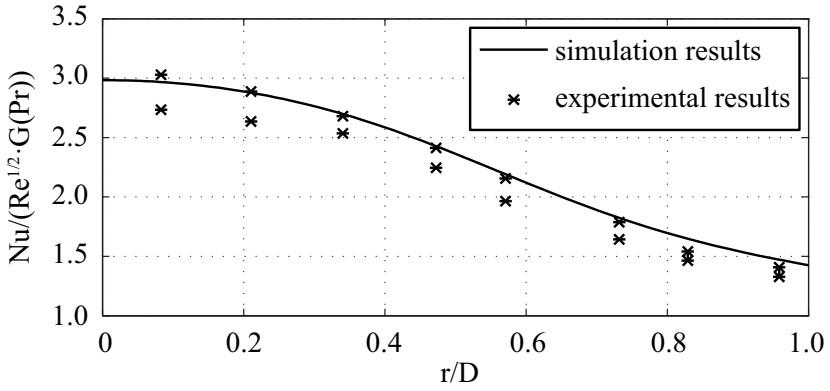

Fig. 4 Validation of the numerical method with experimental data [24]. The experimental data correspond to $Re = 1970$, $H/D = 4$ and $Re = 950$, $H/D = 2$, such that $H/(D{\cdot}Re) \approx 0.002$. In the numerical simulation, a constant temperature boundary condition at the wall has been applied. $G(Pr)$ represents the analytical Prandtl number dependency based on a self-similar solution of the stagnation point flow given in White [28].

3. METHOD VALIDATION

A grid dependence analysis is performed for both configurations. Figure 3 presents the final results of this analysis, showing the local distribution of the Nusselt number. The Nusselt profiles computed with the basic mesh and a mesh refined in all spatial and temporal directions agree well in shape and in absolute value, thereby showing grid independence of the solution. The uncertainty due to discretization was estimated based on the ASME standard [4]. The error of the average Nusselt number in the stagnation zone is evaluated for the highest Prandtl number examined, yielding an approximate relative error of $e_{\mathrm{a}}^{12} = 0.44\%$, an extrapolated relative error of $e_{\mathrm{ext}}^{12} = 0.60\%$, and a fine-grid convergence index of $GCI = 0.22\%$.

For validation of the numerical method, the radial Nusselt profile is compared with experimental data from Scholtz and Trass [24] for the free-surface case. Using an air–naphthalene system (Schmidt number $Sc = 2.45$), the authors obtained local mass transfer rates. The constant concentration boundary condition at the impinging wall corresponds to a constant temperature boundary condition in the equivalent case of heat transfer. The Sherwood number (or equivalent Nusselt number) has been rescaled according to the analytical Prandtl number dependency given in White [28]; see also Rohlfs et al.[19]. Experimental data in Scholtz and Trass are given for different nozzle-to-plate distances ($0.5 \leq H/D \leq 6$) and Reynolds numbers ($800 \leq Re \leq 1970$). Due to the self-similarities in the system [19], the reduced heat transfer coefficient for cases with the same value for $H/(D \cdot Re)$ coincide for sufficiently large nozzle-to-plate distances (H/D). The experimental results for two

different combinations of Re and H/D but with the same $H/(D \cdot Re) = 0.002$ are shown in Fig. 4 with numerical data for the same flow condition, revealing good agreement in both; the shape of the radial distribution and the absolute value.

4. RESULTS

4.1 Hydrodynamics of free jets

The hydrodynamic development of the free jet before impinging on the wall has a substantial influence on the heat transfer and will therefore be discussed in the following section.

For the *submerged case*, the free jet flow is shown in Fig. 5a. According to Viskanta [27], the free jet region can be subdivided into three major zones : the potential core zone, the developing zone, and the developed zone. In the potential core zone, the velocity is unaffected and remains equal to the nozzle exit velocity. In the plot, the potential core region is illustrated by the two iso-velocity lines $0.90 \cdot u_\infty$ and $0.95 \cdot u_\infty$. According to Livingood [11], the length of this zone is 6-7 diameters from the nozzle exit, independent from the Reynolds number. However, the present simulation results for laminar jets (Reynolds number of 540) indicate that this zone can penetrate up to 17 jet diameters. The definition of a potential core zone can only be applied for a uniform velocity profile at the nozzle exit. For a parabolic outlet profile, the center velocity starts to decay at the nozzle exit (see Fig. 5c).

In the developing zone, the axial velocity decays due to the large shear stress at the jet boundary. In the developed zone (after approximately $6D$), the basic shape of the velocity profile is characterized by self-similarity [23]. This profile is best fitted by a Gaussian distribution [27]. Furthermore, a linear behavior is reported in the literature for the jet broadening. Contrary, the present simulation results show that the jet broadening rather follows a parabolic shape.

For the *free-surface case* shown in the center plot, the shear stress at the outer edge of the jet has a negligible influence on the free jet. Thus, only shear forces in the liquid core or gravity can induce a change of the initial velocity profile. The development of a parabolic velocity profile due to viscous relaxation can be observed. The free jet can be subdivided into two major regions: the developing zone and the developed zone.

In the developing zone, the inner core of the jet decelerates while the outer part accelerates. Assuming no loss in mass and momentum, the center velocity (see plot c) decays from $2 \cdot u_\infty$ to $4/3 \cdot u_\infty$, where u_∞ is the average velocity of the parabolic profile. As a result of this acceleration, the jet contracts such that the radius reduces to $\sqrt{3/4} \cdot r$. Self-similarity in the decay can be found by introducing a scaling of $Re \cdot D$, which can be drived from a balance of inertia and viscous forces in axial direction. With this scaling, the axial velocity u_{ax} exponentially decays. This decay can be approximated according to

$$\frac{u_{\mathrm{ax}}}{u_\infty} = \frac{4}{3} + \frac{2}{3} \exp\left(-m \frac{x'}{D \cdot Re}\right). \tag{2}$$

The exponent m can be analytically determined only at the nozzle exit where it takes a value of $m = 24$. Further downstream the exponent increases such that an average decay of $m = 38.9$ gives reasonable agreement with numerical data. After the developing region, the velocity profile of the jet is uniform.

The submerged jet with a parabolic velocity profile at the inlet initially shows the same decay in the centerline velocity up to $x/(D \cdot Re) \approx 0.02$, where the influence of viscous forces, induced by the ambient fluid, becomes relevant. Due to the shear forces, the centerline velocity of the submerged jet decreases continuously, independently from the imposed velocity profile.

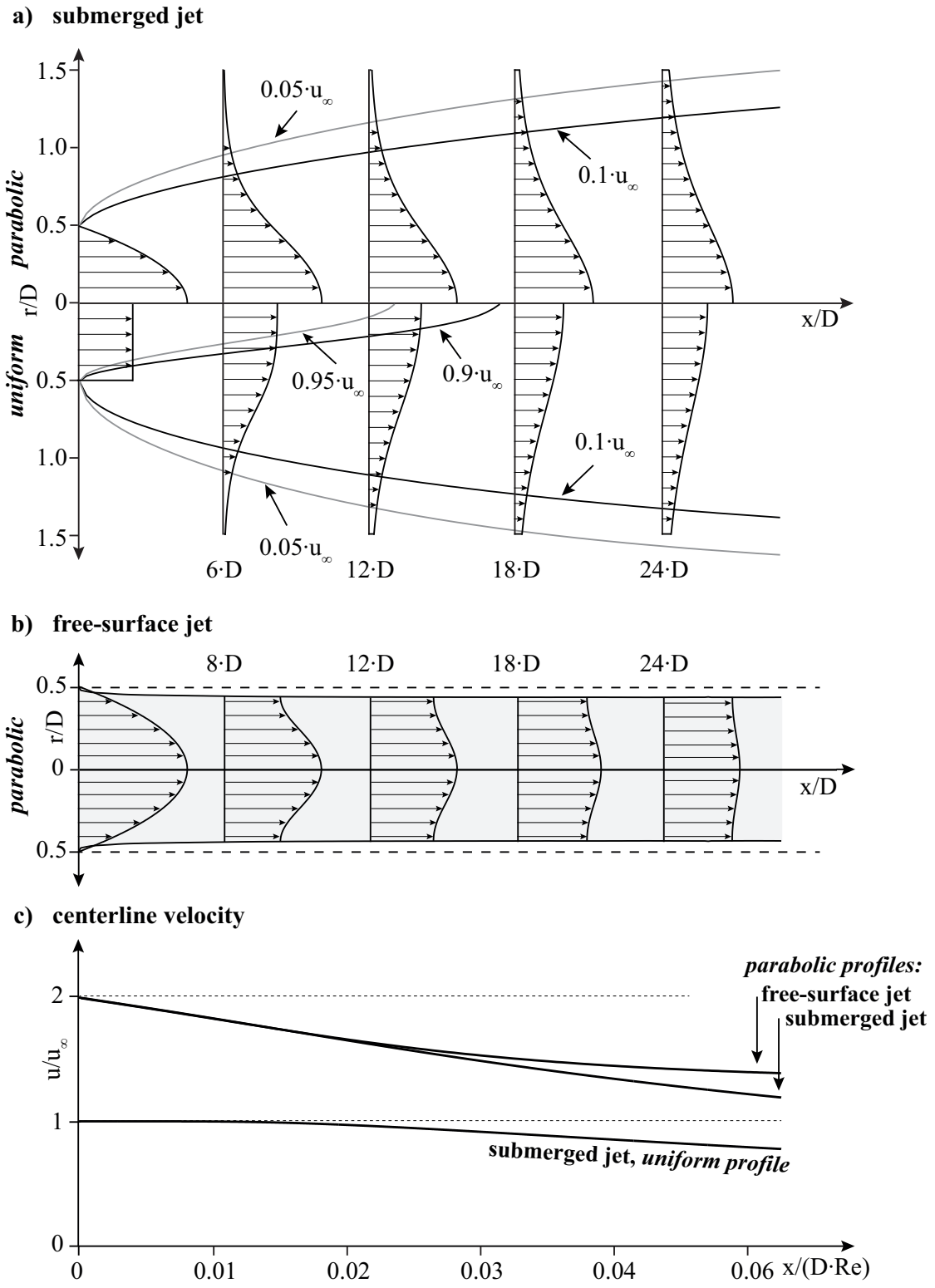

Fig. 5 Velocity profile of free jet flows ($Re = 540$) for the submerged (bottom image) and free-surface configuration (center image). The top image shows the development of the center-line velocity.

4.2 Heat transfer characteristics

The following two subsections present the heat transfer characteristics of submerged and free-surface jets. Thereby, the Nusselt number is defined as follows:

$$\mathrm{Nu}(r) = \frac{\dot{q}(r)}{T_\mathrm{W}(r) - T_\infty} \frac{D}{k}, \tag{3}$$

where k denotes the thermal conductivity, D the nozzle diameter, and $\dot{q}(r)$ the area specific heat flux. For a constant temperature boundary condition, the local heat flux, $\dot{q}(r)$, is evaluated at the wall due to the local temperature gradient. For a constant heat flux boundary condition, the wall temperature, T_W, is evaluated from the results of the numerical simulations

It is important to emphasize that dissipative heat generation is not accounted for in the numerical simulations. Thus, the Nusselt number estimated based on the wall temperature is equivalent to the Nusselt number based on the adiabatic wall temperature in experiments.

4.2.1 Submerged jet configuration The distribution of the local dimensionless heat transfer coefficient at the wall for the submerged jet configuration is shown in Fig. 6. The figure includes a variation of the Reynolds number, the inlet velocity profile and the boundary condition at the impingement wall while a constant water-like Prandtl number ($Pr = 7$) and a constant nozzle-to-plate distance ($H/D = 4.5$) have been imposed. A similar plot for $Pr = 0.7$ is shown in an earlier study [20], revealing good agreement with experimental data. For the parabolic velocity profile, the Nusselt number distribution is characterized by a monotonically decaying trend, showing a general increase with Reynolds number. For the uniform velocity profile, the Nusselt number distribution increases from the centerline to a local maximum at $r/d \approx 0.6$. For larger radii, the Nusselt number decreases similar to the parabolic velocity profile. The causing effect of the local maximum will be discussed in subsection 4.3. A direct comparison of the two profiles reveals that the stagnation point Nusselt number is more than twice as high for the parabolic case as for the uniform velocity profile, due to a higher velocity at the center of the incoming jet. For both velocity profiles, the thermal boundary condition at the wall does not influence the heat transfer at the stagnation point. However, further away from the stagnation point, a constant wall temperature is found to result in a faster decay of the Nusselt number compared to a constant heat flux. These findings agree qualitatively with analytical results for boundary layer flows over a flat plate or in thermally developed pipe flows [2], although the magnitude of the difference depends on the exact velocity profile and its development. Note that the local off-center peak is more dominant for the constant wall temperature.

4.2.2 Free-surface jet configuration In analogy to the numerical experiments performed for the submerged jet, the Nusselt number distribution for free-surface jet impingement has been investigated. Figure 7 shows the influence of the Reynolds number for a constant Prandtl number ($Pr = 7$) and a constant nozzle-to-plate distance ($H/D = 55$). A parabolic velocity profile has been applied to the nozzle exit. Similar to the previous results, the Nusselt number distribution reveals a generally decreasing trend in radial direction. However, for low Reynolds numbers an off-center peak at $r/D \approx 0.6$ exists, while for higher Reynolds numbers this peak vanishes leading to a global maximum at the centerline. This strong Reynolds dependency on the shape of the Nusselt distribution has not been observed for the submerged jet. The significant change of the shape can be explained with the assistance of the previous results. As mentioned before, the impingement of a uniform velocity profile is found to cause the off-center peak, contrary to a parabolic velocity profile. Although, a parabolic velocity profile is imposed at the nozzle exit of the free-surface configuration, this profile relaxes, while travelling to the impingement wall, into a more uniform velocity profile (see subsection 4.1). The progress of the relaxation depends on the dimensionless distance $x/(D \cdot Re)$. Therefore, the velocity profile near the impingement wall is more uniform, the lower the Reynolds number is. Thus, a local off-center

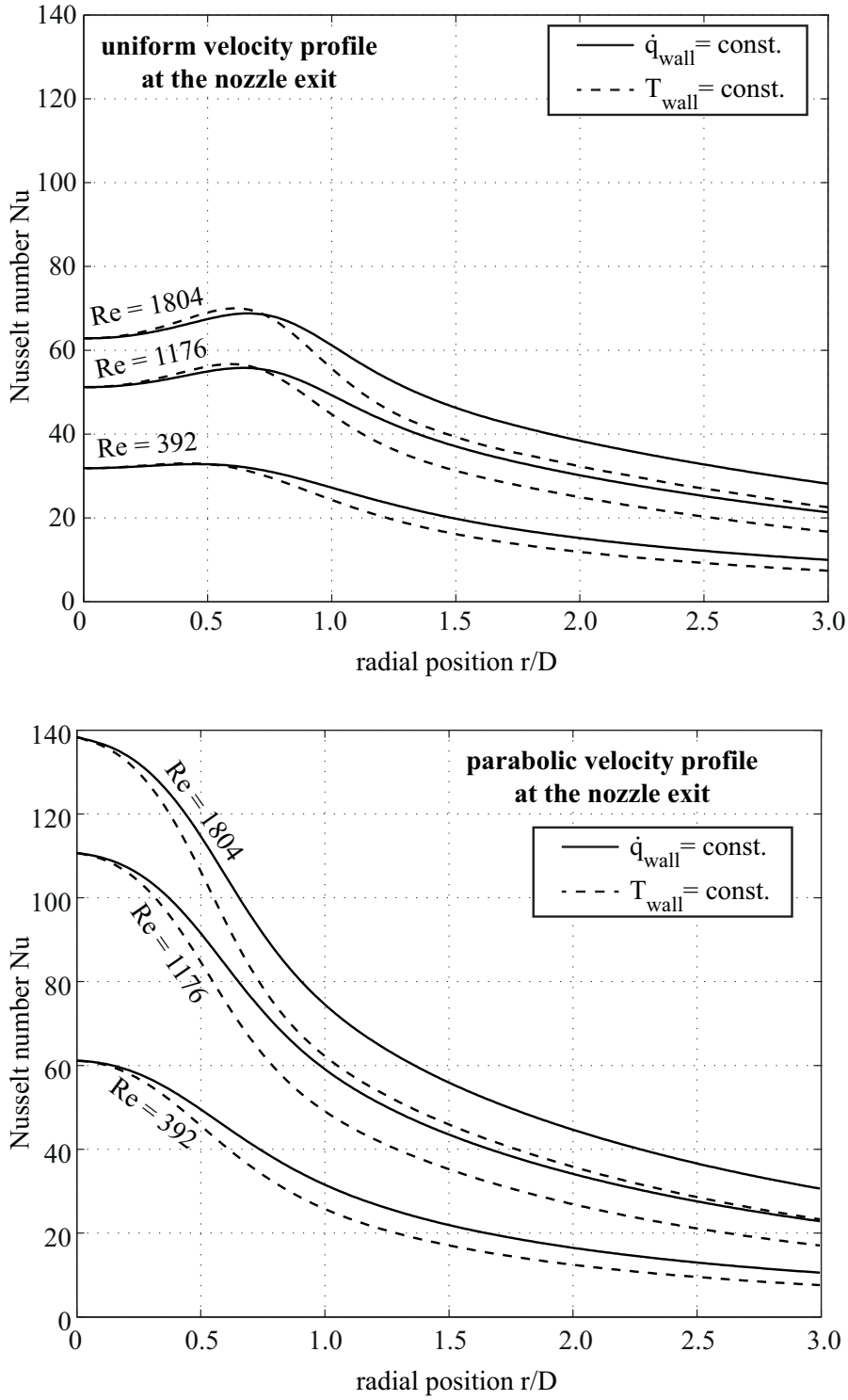

Fig. 6 Distribution of the local Nusselt number for a *submerged* jet with a constant Prandtl number of $Pr = 7$ and a constant nozzle-to-plate distance $H/D = 4.5$.

peak can be observed for low Reynolds numbers while a centerline peak occurs for high Reynolds numbers. Consequently, the Reynolds number for the transition between centerline and off-center peak depends on the nozzle-to-plate distance, which is constant for the results presented. Additional simulations with different values for the geometric parameter H/D have verified the influence of the scaling factor on the shape of the Nusselt profile.

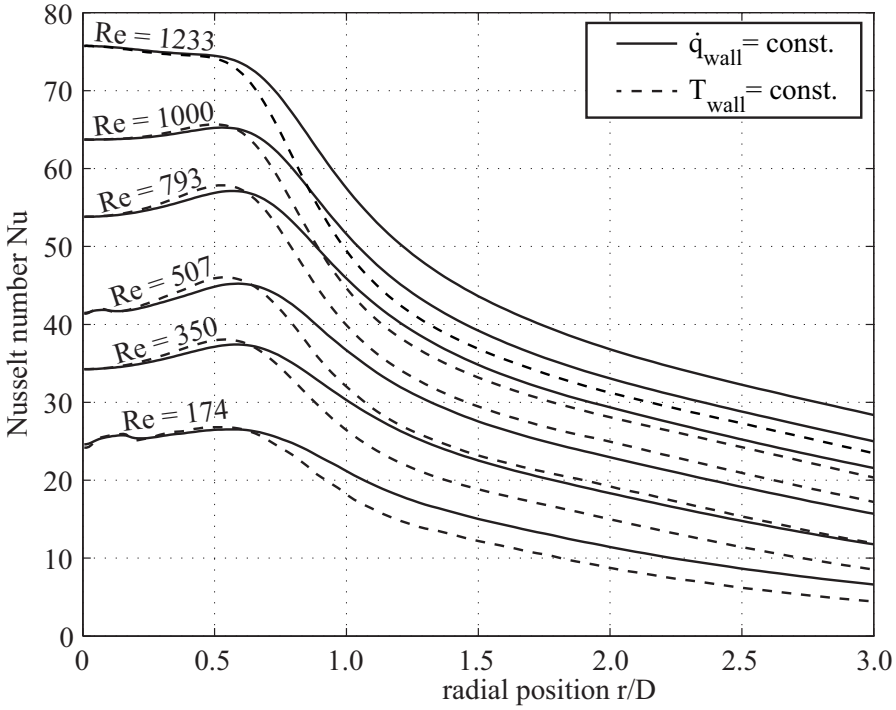

Fig. 7 Distribution of the local Nusselt number for *free-surface* jets with a nozzle-to plate distance of $H/D = 55$ and a parabolic velocity profile at the nozzle exit. Influence of Reynolds number for $Pr = 7$.

4.3 Influence of local flow acceleration

For investigating the causing effect of the change in the Nusselt profile between $Re = 1000$ and $Re = 1233$, i.e. the appearance of an off-center peak in the free-surface jet case, the velocity, pressure, and temperature fields in the stagnation region have been closely examined. Note that a similar method was followed by the authors for the submerged jet configuration [20]. Due to the relevance of those findings to the present results some of the explanations will be recalled here. Figure 8(a) compares the two velocity profiles in radial direction at a wall distance of $2D$, where the jet velocity is not yet influenced by the presence of the impingement wall. These profiles (normalized by the mean jet velocity, $\overline{u}_\infty$) deviate significantly from the parabolic profile imposed at the nozzle exit (inlet of the computational domain) caused by relaxation following the loss of the shear force at the jet's boundary [16]. In order to preserve the kinetic energy the average velocity increases and due to continuity the jet contracts. In the centerline, the axial velocity $u/\overline{u}_\infty$ in the near wall region for $Re = 1233$ is higher than for $Re = 1000$ (solid line). This is reflected in the pressure distribution on the wall in the stagnation region (see Fig. 8b), where the center value of the pressure profile and the pressure gradient $\partial p/\partial r$ are also higher for $Re = 1233$ (but only 3.2%). Further downstream in the radial direction ($r/D > 0.5$), both curves converge. This pressure distribution directly influences the gradient of the radial velocity ($\partial(uD)/\partial(r\overline{u}_\infty)$) in the near wall region, see Fig. 8c. For $Re = 1233$, a high radial acceleration is observed in the center of the jet from where it monotonously decays in radial direction, reaching its minimum at $r/D \approx 0.8$. In contrast, the local acceleration for a more relaxed velocity profile *increases* in radial direction up to a maximum at a distance of $r/D \approx 0.5$. Mass conservation requires a compensation for the high radial acceleration ($\partial u/\partial r$)

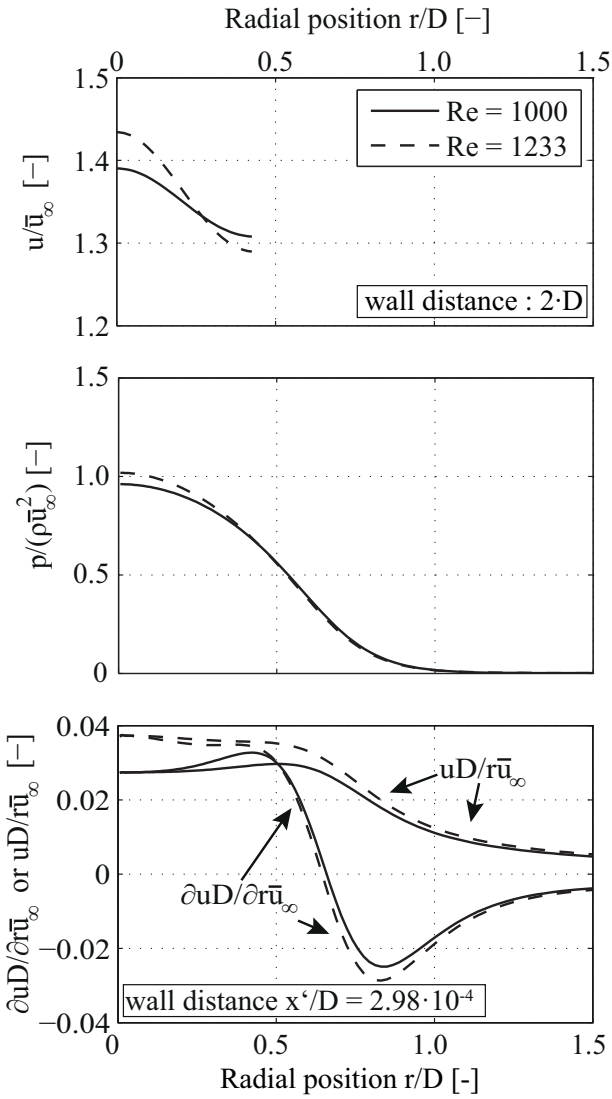

(a) Profile of the axial velocity of the jet at a wall distance 2·D.

(b) Dimensionless pressure distribution on the impinging wall.

(c) Gradient of the dimensionless radial velocity near the wall.

Fig. 8 Influence of the approaching velocity profile on the pressure distribution at the wall and the radial acceleration.

and for the increasing cross sectional area in radial direction u/r. This results in a velocity gradient in the direction normal to the wall, $(\partial v/\partial x)$, which causes an inflow normal to the wall, as illustrated in Fig. 9a. The Nusselt number distribution (Fig. 9c) shows the appearance of a peak at $r/D \approx 0.5$ for $Re = 1000$, while for $Re = 1233$ the profile monotonically decreases.

Comparing the near wall velocity with the Nusselt number distribution (Fig. 9, a and c), strong similarities can be observed. In both plots, a Reynolds number of $Re = 1233$ leads to a monotonically decreasing behavior for $r/D < 0.75$, whereas for $Re = 1000$, both plots depict a global maximum in the range $0.5 < r/D < 0.75$. The strongest inflow and consequently the strongest transport of cold fluid to the wall for $Re = 1233$ is found at the centerline of the jet, leading to a maximum in heat transfer at the stagnation point ($\mathrm{Nu}_{\mathrm{stag.}} = 313$). By contrast, the local minimum of the axial velocity at the centerline for $Re = 1000$ leads to a local minimum in heat transfer coefficient ($\mathrm{Nu}_{\mathrm{stag.}} = 263$). As first introduced in the earlier study of the authors [20], a critical value for the magnitude of this inflow velocity, required for generating a decreasing wall temperature in the radial direction and consequently an inner peak in the Nusselt number, was derived based on a steady state

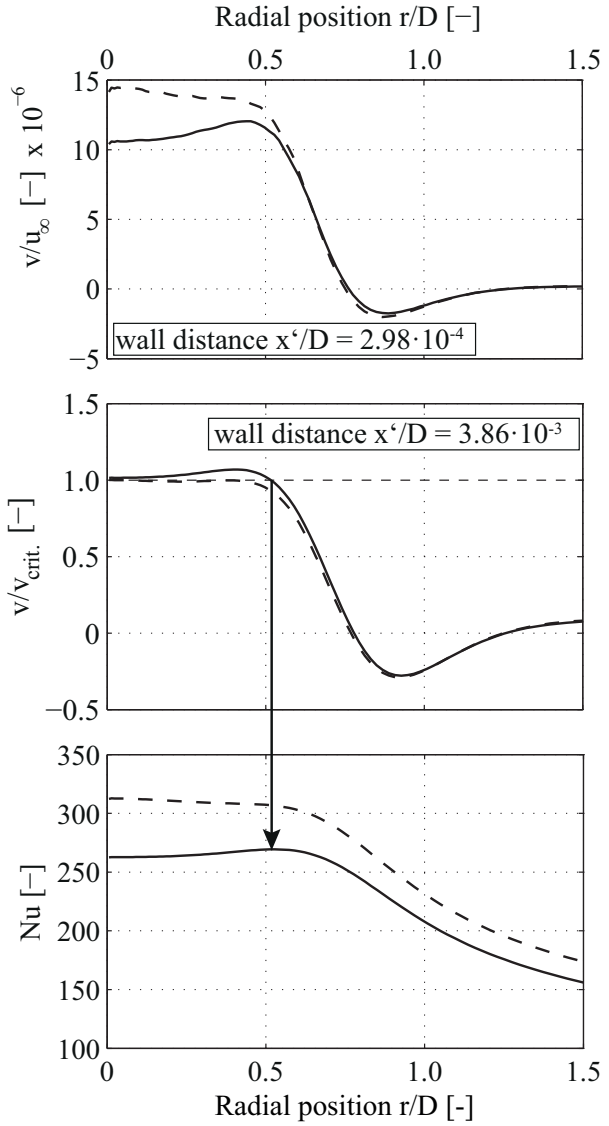

(a) Dimensionless axial velocity near the wall.

(b) Ratio between axial velocity and the critical velocity.

(c) Nusselt number distribution

Fig. 9 Correlation between the occurrence of an inner peak in the radial distribution of the Nusselt number and the axial velocity.

energy balance analysis near the wall, as:

$$v_{\text{crit}} = \frac{k}{\rho c_p} \frac{\partial^2 T(r,x)}{\partial x^2} \frac{1}{\frac{\partial T(r,x)}{\partial x}} \ , \tag{4}$$

where a condition of $v > v_{\text{crit}}$ will lead to an increase of the heat transfer coefficient in flow direction and thus to the emergence of an off-center peak. However, this critical velocity is dependent on the ratio between the first and the second derivative of the near wall temperature, thereby it is an a-posteriori condition and thus can not predict the appearance of an off-center peak based on nominal flow conditions. In order to evaluate the critical velocity, the temperature field of the numerical simulation was used to calculate the first and second derivative. As both, the second derivative and the normal velocity, v, disappear at the wall, they are evaluated very close to the wall. The ratio between actual and critical axial velocity, v/v_{crit} is depicted in Fig. 9b. The velocity, resulting from the more relaxed velocity profile, is seen to surpass the critical value (indicated by the dashed line) in the range of $r/D < 0.52$. The radial position, at which the velocity then crosses this criterion, coincides with the region of highest Nusselt number as indicated by the arrow running from Fig. 9(b and c).

The near-wall normal velocity for $Re = 1233$ stays below this criterion for all radial positions and thus no peak is observed.

The findings presented in this subsection reveal that the velocity profile which approaches the wall dictates the appearance of an off-center peak not only for submerged jets [20], but also for the case of free-surface jets.

5. CONCLUSION

In the present study, the heat transfer mechanisms of submerged and free-surface jet impingement have been investigated using fully resolved numerical simulations. The numerical methods have been validated by a grid dependency analysis and by a comparison to experimental results. In the free jet region, where the jet is not yet influenced by the presence of the impingement wall, the development of the velocity profile of the two cases (submerged and free-surface jet) differs significantly outside the potential core region. However, very strong similarities exist in the radial distribution of the heat transfer coefficient in the stagnation region. Consequently, the effect of the first local peak in the distribution of the heat transfer coefficient which is well known for submerged jets is also present under specific conditions of free-surface jet impingement. This local peak is caused by local flow acceleration and is strongly coupled to the impinging velocity profile, which has to be of uniform type in order to generate an increasing heat transfer coefficient in radial direction. This type of velocity profile exists in case of submerged jets for low nozzle-to-plate distances and orifice-type nozzles. Contrary, in case of free-surface jets, the effect of viscous relaxation unifies the velocity profile for long nozzle-to-plate distances for which a local peak can be observed.

ACKNOWLEDGMENTS

We gratefully acknowledge the financial support from the Deutsche Forschungsgemeinschaft (grant number DFG KN 764/3-2).

REFERENCES

[1] Barsanti, G., Faggiani, S., and Grassi, W., "Single-phase foced convection cooling of heating surfaces by liquid jet impingement," *Int. J. Heat and Technology*, 7, pp. 1–11, (1989).

[2] Beahr, H. D. and Stephan, K., *Heat and Mass Transfer*, Springer Berlin / Heidelberg, (2006).

[3] Brackbill, J., Kothe, D., and Zemach, C., "A continuum method for modeling surface tension," *J. of Computational Physics*, 100, pp. 335–354, (1992).

[4] Celik, I. B., Ghia, U., Roache, P. J., Freitas, C. J., Coleman, H., and Raad, P. E., "Procedure for Estimation and Reporting of Uncertainty Due to Discretization in CFD Applications," *J. Fluids Eng.*, 130, pp. –, (2008).

[5] Gardon, R. and Akfirat, J., "The role of turbulence in determining the heat-transfer characteristics of impinging jets," *Int. J. of Heat and Mass Transfer*, 8(10), pp. 1261 – 1272, (1965).

[6] Grassi, W. and Magrini, A., "Effect of the free jet fluid-dynamics on liquid jet impingement heat transfer," *9th National Heat Transfer Conference of Italy*, (1991).

[7] Hirt, C. W. and Nichols, B. D., "Volume of fluid (VOF) method for the dynamics of free boundaries," *J. of Computational Physics*, 39, pp. 201–225, (1981).

[8] Kataoka, K., Suguro, M., Degawa, H., Maruo, K., and Mihata, I., "The effect of surface renewal due to largescale eddies on jet impingement heat transfer," *Int. J. of Heat and Mass Transfer*, 30(3), pp. 559 – 567, (1987).

[9] Kezios, S. P., Heat transfer in the flow of a cylindrical air jet normal to an infinite plane, PhD thesis, Illinois Institute of Technology, (1956).

[10] Liu, X. and Lienhard, J. H., "Liquid jet impingement heat transfer on a uniform flux surface," *Heat Transfer Phenomena in Radiation, Combustion, and Fires*, (1989).

[11] Livingood, J. N. B. and Hrycak, P., "Impingement heat transfer from turbulent air stream jets to flat plates – a literature survey," , Tech. rep., NASA Technical Memorandum, (1973). NASA TM X-2778.

[12] Lytle, D. and Webb, B., "Air jet impingement heat transfer at low nozzle-plate spacings," *Int*, 37(12), pp. 1687 – 1697, (1994).

[13] Ma, C., Zhao, Y., Masuoka, T., and Gomi, T., "Analytical study on impingement heat transfer with single-phase free-surface circular liquid jets," *J. of Thermal Science*, 5(4), pp. 271–277, (1996).

[14] Martin, H., "Heat and mass transfer between impinging gas jets and solid surfaces," *Advances in Heat Transfer*, 13, pp. 1–60, (1977).

[15] Pamadi, B. and Belov, I., "A note on the heat transfer characteristics of circular impinging jet," *Int. J. of Heat and Mass Transfer*, 23(6), pp. 783 – 787, (1980).

[16] Philippe, C. and Dumargue, P., "Étude de l'établissement d'un jet liquide laminaire émergeant d'une conduite cylindrique verticale semi-infinie et soumis à l'influence de la gravité," *Zeitschrift für angewandte Mathematik und Physik ZAMP*, 42(2), pp. 227–242, (1991).

[17] Polat, S., Huang, B., Mujumdar, A. S., and Douglas, W. J. M., "Numerical flow and heat transfer under impinging jets: A review," *Annual Review of Heat Transfer*, 2, pp. 157–197, (1989).

[18] Popiel, C. O., van der Meer, T. H., and Hoogendoorn, C., "Convective heat transfer on a plate in an impinging round hot gas jet of low Reynolds number," *Int. J. of Heat and Mass Transfer*, 23(8), pp. 1055 – 1068, (1980).

[19] Rohlfs, W., Ehrenpreis, C., Haustein, H. D., and Kneer, R., "Self-similarity in free-surface impinging jets: Viscous flow relaxation and its influence on maxima of local heat transfer," *Under consideration for publication in Int. J. of Heat and Mass Transfer*, pp. –, (2014).

[20] Rohlfs, W., Haustein, H. D., Garbrecht, O., and Kneer, R., "Insights into the local heat transfer of a submerged impinging jet: Influence of local flow acceleration and vortex-wall interaction," *Int. J. of Heat and Mass Transfer*, 55(2526), pp. 7728 – 7736, (2012).

[21] Rusche, H., Computational fluid dynamics of dispersed two-phase flows at high phase fractions, PhD thesis, Imperial Collage, University of London, (2002).

[22] Saad, N. R., Douglas, W. J. M., and Mujumdar, A. S., "Prediction of heat transfer under an axisymmetric laminar impinging jet," *Industrial & Engineering Chemistry Fundamentals*, 16(1), pp. 148–154, (1977).

[23] Schlichting, H. and Gersten, K., *Boundary Layer Theory*, Springer Berlin / Heidelberg, (2000).

[24] Scholtz, M. T. and Trass, O., "Mass transfer in a nonuniform impinging jet," *AIChE Journal*, 16(1), pp. 82–96, (1970).

[25] Sparrow, E. M. and Lovell, B. J., "Heat transfer characteristics of an obliquely impinging circular jet," *J. of Heat Transfer*, 102(2), pp. 202–209, (1980).

[26] Stevens, J. and Webb, B. W., "Local heat transfer coefficients under an axisymmetric, single-phase liquid jet," *J. of Heat Transfer*, 113(1), pp. 71–78, (1991).

[27] Viskanta, R., "Heat transfer to impinging isothermal gas and flame jets," *Experimental Thermal and Fluid Science*, 6(2), pp. 111 – 134, (1993).

[28] White, F. M., *Viscous Fluid Flow*, 2nd Edition, McGraw-Hill, New York, (1991), chapter 3-8.

[29] Zuckerman, N. and Lior, N., "Jet impingement heat transfer: Physics, correlations, and numerical modeling," *Advances in heat transfer*, 39, pp. 565–631, (2006).